

A new Einstein Cross gravitational lens of a Lyman-break galaxy

DANIELA BETTONI,¹ RENATO FALOMO,¹ RICCARDO SCARPA,² MATTIA NEGRELLO,³ ALESSANDO OMIZZOLO,^{4,1}
ROMANO L. M. CORRADI,² DANIEL REVERTE,² AND BENEDETTA VULCANI¹

¹*INAF - Osservatorio Astronomico di Padova, Vicolo Osservatorio 5 35122 Padova, Italy*

²*GRANTECAN, Cuesta de San José s/n, E-38712, Breña Baja, La Palma, Spain, Instituto de Astrofísica de Canarias, Vía Láctea s/n, E38200, La Laguna, Tenerife, Spain*

³*School of Physics and Astronomy, Cardiff University, The Parade, Cardiff CF24 3AA, UK*

⁴*Vatican Observatory, Vatican City State, Vatican City*

(Received XX, 2019; Revised XX, 2019; Accepted March 1, 2019)

Submitted to ApJLett

ABSTRACT

We report the study of an "Einstein Cross" configuration first identified in a set of HST images by Cerny et al. (2018). Deep spectroscopic observations obtained at the Spanish 10.4m GTC telescope, allowed us to demonstrate the lens nature of the system, that consists of a Lyman-break galaxy, not a QSO as is usually the case, at $z = 3.03$ lensed by a galaxy at $z=0.556$. Combining the new spectroscopy with the archival HST data, it turns out that the lens is an elliptical galaxy with $M_V = -21.0$, effective radius 2.8 kpc and stellar velocity dispersion $\sigma=208\pm39$ km/sec. The source is a Lyman break galaxy with Ly α luminosity $\sim L^*$ at that redshift. From the modeling of the system, performed by assuming a singular isothermal ellipsoid (SIE) with external shear, we estimate that the flux source is magnified about 4.5 times, and the velocity dispersion of the lens is $\sigma_{\text{SIE}} = 197.9_{-1.3}^{+2.6}$ km s⁻¹, in good agreement with the value derived spectroscopically. This is the second case known of an Einstein cross of a Lyman-break galaxy.

Keywords: gravitational lensing – galaxies: elliptical, high redshift — techniques: spectroscopic

1. INTRODUCTION

Gravitational lenses represent one of the most powerful tool to probe the properties of distant galaxies and the cosmological parameters. Strong gravitational lensing produces multiple images of distant sources that have their line of sight very close to foreground massive objects (see Treu 2010, for a review). In addition the special case of image splitting of distant quasars can provide the direct measurement of the Hubble constant from correlated flux variability (Treu and Koopmans 2002; Suyu et al. 2014).

Accurate lens modelling can precisely probe the density profile of galaxies at cosmological distances, specifically the mass enclosed within the Einstein radius and the mean local density slope within it. Combining lensing and dynamics allows the central dark matter profile

to be robustly inferred (e.g. Treu and Koopmans 2004). All these facts make this kind of configuration a fantastic laboratory for the study of the Universe.

Of particular interest is the detection of quadruple images of lensed QSO in the shape of an Einstein Cross (see e.g. Wisotzki et al. (2002); Morgan et al. (2004) for first discoveries). However, these optical structures are rare on the sky (Oguri and Marshall 2010) as they require a very close alignment of quasars with foreground massive galaxies. Various large-area sky surveys are planned in the near future to increase the number of such systems (e.g. Williams et al. 2017, 2018; Schechter et al 2017; Agnello et al. 2018) and recently the H0LiCOW (H₀ Lenses in COSMO-GRILs Wellspring) program (Suyu et al. 2017; Bonvin et al. 2017) listed the five best lensed quasars discovered to date showing an Einstein Cross structure.

During a search for high z galaxies from the Reionization Lensing Cluster Survey (RELICS) of the Hubble Treasury Program (Salmon et al. 2017), a possible new

Einstein Cross configuration around a galaxy located at $\alpha = 22:11:41.99$, $\delta = 03:50:52.3$ was discovered by Cerny et al. (2018) (see Figure 1). Later on, during a search for stripped galaxies in the HST images from the RELICS project, the serendipitously re-discovery of this object by one of us (A.O.) led to the observations presented in this article. The system, hereafter called J2211-0350, is sitting ~ 90 arcsecs South-West from the core of the cluster RXC J2211.7-0349 ($z=0.397$) and, based on the redder color of the alleged lens galaxy, it was argued that the lens had to be well behind the nearby cluster. The system is composed by an early-type red galaxy surrounded by 4 blue objects which are arranged in the shape of a "Latin Cross" around the central galaxy. In Table 1 we report the magnitudes and the relative positions of the image components. Data are from the RELICS catalogs except for the component D that we measured directly on the HST images.

Prompted by this discovery we report here the results of optical spectroscopy of the system that allows us to confirm its lensing nature and measure the redshift of both the lens and the source. We adopt the concordance cosmology and assume $H_0 = 70 \text{ km s}^{-1} \text{ Mpc}^{-1}$, $\Omega_m = 0.3$ and $\Omega_\Lambda = 0.7$.

2. OBSERVATIONS AND DATA ANALYSIS

Spectroscopic observations were collected on December 1 2018 at the 10.4 m Gran Telescopio Canarias (GTC), located at the Roque de Los Muchachos observatory, La Palma (Spain). We used the optical spectrograph OSIRIS (Cepa et al. 2003) with the grism R1000B covering the spectral range 4100–7500 Å, and a slit width of 1.0 arcsec. This configuration yields an effective spectral resolution of $R \sim 600$.

Fig. 1 shows an HST image of the target with superimposed the position of the slit, located so to observe both the lensing galaxy and the three brighter images of the source at once. Only source D is outside the slit. Three independent exposures of 1800 sec were obtained under photometric conditions and good atmospheric seeing (0.8 arcsecs).

Standard IRAF¹ tools were adopted for the data reduction. Bias subtraction, flat field correction, image alignment and combination were performed. Cosmic rays were cleaned by combining the three independent exposures and using the *crreject* algorithm. The spectra were then calibrated in wavelength with $\sim 0.2 \text{ \AA}$ accu-

¹ IRAF is distributed by the National Optical Astronomy Observatory, which is operated by the Association of Universities for Research in Astronomy (AURA) under cooperative agreement with the National Science Foundation

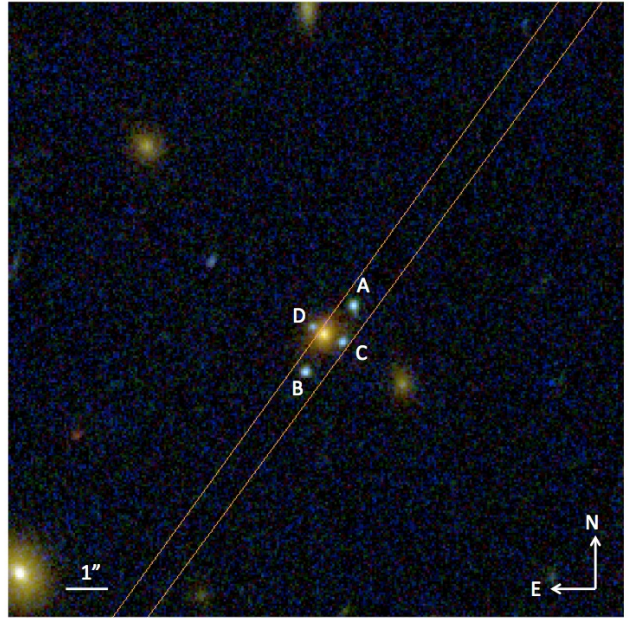


Figure 1. HST color image of the new Einstein Cross J2211-0350 in the field of the cluster RXC J2211.7-0349. The image is a combination of WFC3/IR (F160W) in red, ACS image (F814W) in green and (F435W) in blue. The orange lines represent the position of the 1-arcsec slit used for the spectroscopic observations. Both the lens galaxy and three lensed targets are observed at once.

racy. Data of a spectrophotometric standard star observed on the same night were used to perform a relative flux calibration of the spectrum. HST photometry on filter F606W was then used to achieve absolute flux calibration of the spectrum (see Table 1).

The final 2d spectrum is characterized by the strong emission from three blobs coincident with the spatial location in the slit of the three lensed sources (see Figure 2 and 3). This leaves no doubt about the nature of this source. The emission, centered at $\lambda = 4904 \text{ \AA}$ is identified as the $\text{Ly}\alpha$ at $z = 3.03$. No other clear emission lines are visible (see Figure 4) implying that the lensed source is a Lyman Break Galaxy (LBG) rather than a QSO. The identification of this line is secure since there are no other emission lines and its profile shows a classic, asymmetric, blue self-absorbed morphology that is typical of $\text{Ly}\alpha$ emission (Jones et al. 2012).

3. RESULTS

The flux and shape of the $\text{Ly}\alpha$ emission for the three blobs are very similar, the observed FWHM for this line is 10-12 Å corresponding to a velocity of $\sim 1200 \text{ km/s}$ at rest frame (Fig. 3, and 5).

The observed flux is $2.4 \times 10^{-16} \text{ erg cm}^{-2} \text{ s}^{-1}$. Including the contribution of source D (estimated from

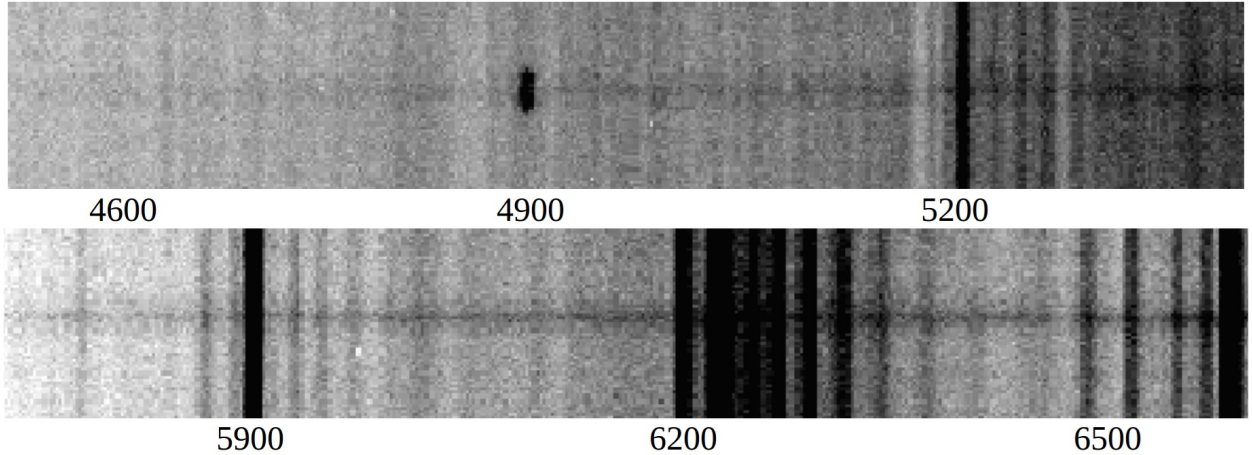


Figure 2. The 2D optical spectrum of the Einstein cross J2211-0350 (see also Fig 3). Superimposed to the faint continuum is a prominent emission line at ~ 4900 Å identified as Ly α .

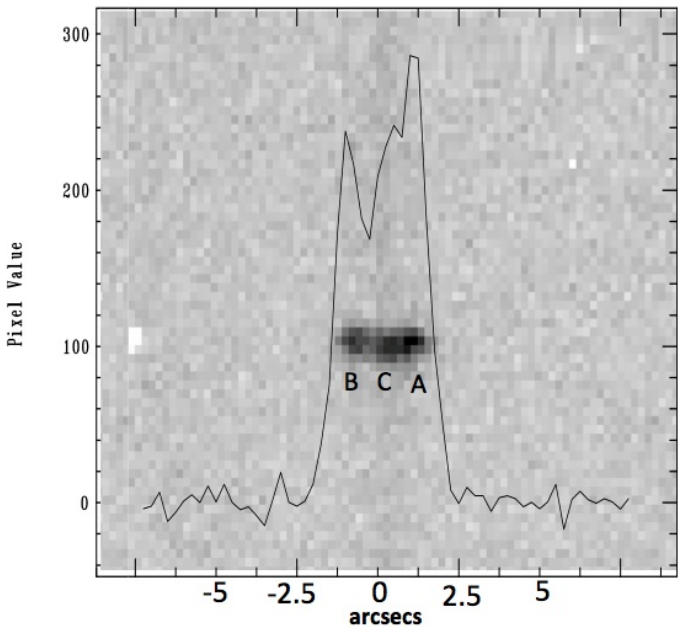


Figure 3. Enlargement of the region around the Ly α . The Ly α emission of the three lensed images (A, B and C) is clearly resolved. Note the slight offset of component C with respect to A and B due to the different position inside the slit (see also Figure 1). The run of the flux along the spatial direction is also shown (solid line).

the HST photometry), we derive a total observed line luminosity of $L(\text{Ly}\alpha) = 2.5 \times 10^{43} \text{ erg s}^{-1}$.

The red part of the spectrum is dominated by the signal from the lens galaxy. Using the pPXF (Cappellari & Emsellem 2004) IDL routines we measured the stellar

Table 1. Position and measured magnitudes

Id.	$\Delta\alpha$	$\Delta\delta$	F435W	F606W	F814W
	arcsec*	arcsec*	AB	AB	AB
Gal	0	0	24.61 ± 0.08	22.83 ± 0.01	21.59 ± 0.01
A	0.826	-0.756	24.80 ± 0.06	24.21 ± 0.02	24.19 ± 0.03
B	-0.481	1.021	24.88 ± 0.06	24.38 ± 0.02	24.25 ± 0.03
C	0.517	0.210	25.24 ± 0.06	24.69 ± 0.02	24.54 ± 0.03
D	-0.324	-0.216	25.7 ± 0.10	25.20 ± 0.15	25.11 ± 0.10

*Positions relative to the lensing galaxy center.

RA(2000) = 22 11 41.97 DEC(2000) = -03 50 52.0

velocity dispersion. The CaII H and K absorption lines were fitted at $z = 0.556$ to estimate the galaxy velocity dispersion. We used the library of single stellar population spectra from Vazdekis et al. (2012) properly convolved with the instrumental resolution to fit the lines profile. The best fit corresponds to a velocity dispersion $\sigma = 208 \pm 39 \text{ km/sec}$. These results confirm the photometric redshift found by Cerny et al. (2018) and that the galaxy is not a member of the cluster RXC J2211.7-0349.

The ACS+F814W image was used to derive the properties of the lensing galaxy. After properly masking the four images of the source, we modeled the lens galaxy with a Sersic law. The data were deconvolved using as PSF an unsaturated and isolated star present in the field. We found that the lens galaxy is well fitted by a model with $n=5$ and effective radius $r_e = 0.44 \text{ arcsec}$ corresponding to $R_e \sim 2.8 \text{ kpc}$. The absolute magnitude of the lens galaxy ($z=0.556$) corresponds to $M_V \sim -21.0$ (taking into account k-correction). The mass of the lens galaxy estimated from the measured σ and R_e is $M_{gal} = 4.5 \times 10^{10} M_\odot$.

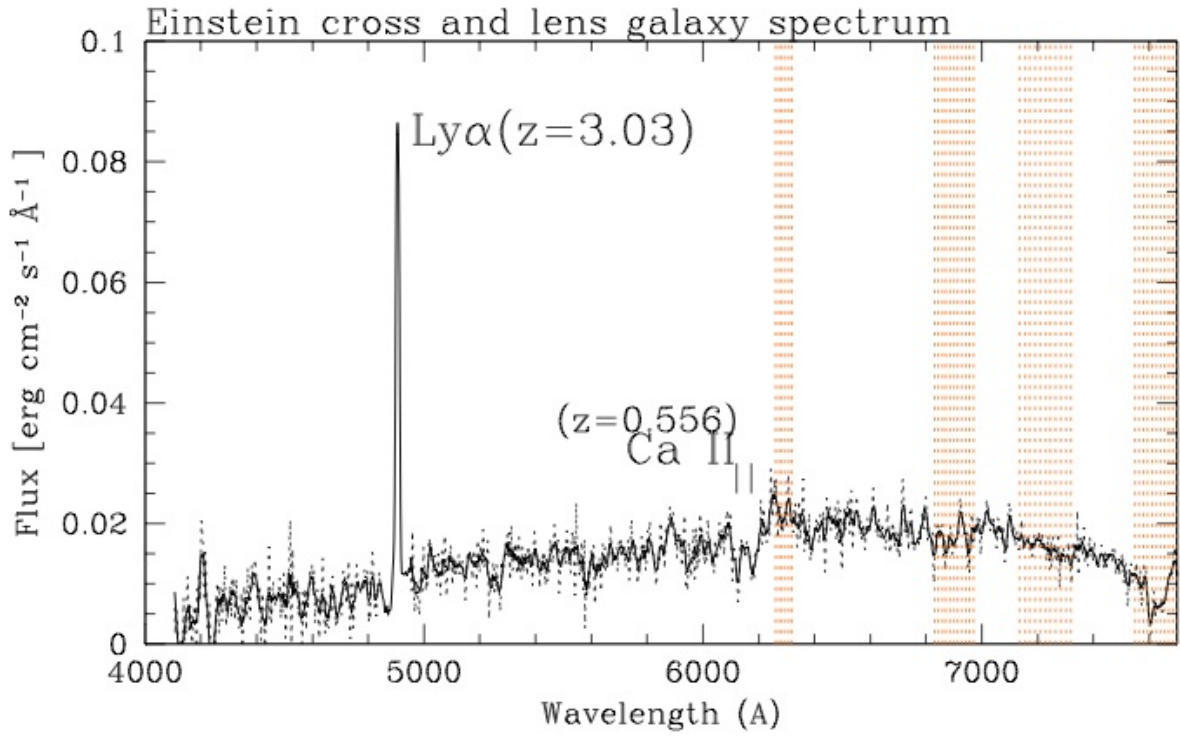


Figure 4. The optical spectrum of the Einstein cross (**observed frame**). This 1D spectrum was obtained by integrating the flux of both the lens galaxy and three lensed images (see also Fig 2). A prominent Ly α emission is visible at $z = 3.03$ due to the lensed source while stellar absorption lines at $z = 0.556$ are due to the lensing galaxy. The regions affected by telluric absorptions are marked (orange vertical lines).

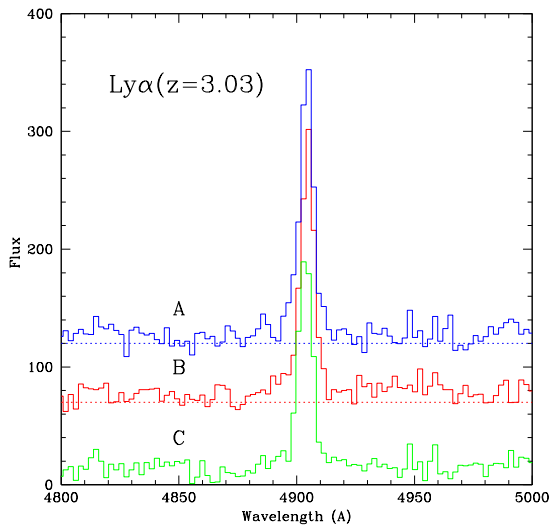


Figure 5. The Ly α region of optical spectrum of the three images of the Einstein cross shifted of an arbitrary quantity to viewing purposes. The peak are labeled a in Fig. 3.

3.1. Lens modeling

We performed the lens modeling of the system by using the code by [Enia et al. \(2018\)](#), which implements the regularized semi-linear inversion formalism with adaptive pixel scale ([Warren & Dye 2003](#); [Suyu et al. 2006](#); [Nightingale & Dye 2015](#), and references therein).

The source plane (SP, i.e. the plane orthogonal to the line-of-sight of the observer to the deflector, containing the background source) is gridded into pixels whose values represent the source surface brightness counts and are treated as free parameters. This approach avoids any a priori analytic assumption on the surface brightness of the background source. The size of the pixels adapts to the magnification pattern, being smaller closer to the regions of increasing magnification, to ensure a uniform signal-to-noise across the reconstructed source and to fully exploit the increase in spatial resolution in highly magnified regions provided by gravitational lensing. For a fixed mass model of the deflector (or lens), the SP is mapped into the image plane (IP, i.e. the plane containing the deflector and orthogonal to the line-of-sight of the observer to the deflector), then convolved with the point spread function, and finally compared to the observed image. In order to avoid unphysical solutions, in with the reconstructed source presenting severe discontinuities and pixel-to-pixel variations, a *regularization term* is added to the merit function. The weight of the

regularization term is calculated via Bayesian analysis, according to [Suyu et al. \(2006\)](#).

The mass distribution of the lens is modeled as a singular isothermal ellipsoid (SIE), described by the following parameters: the Einstein radius (θ_E), the position of the lens centroid (x_L, y_L), the minor-to-major axis ratio (q_L), the orientation angle (θ_L ; counter-clockwise from west). Although the object is at the edge of the nearby cluster, to model the lens, an external shear is included in the model. It is described by the shear strength (γ) and the shear angle (θ_γ ; counter-clockwise from west). The search for the best-fitting parameters of the lens is done using the EMCEE code ([Foreman-Mackey et al. 2012](#)), which implements the Markov chain Monte Carlo (MCMC) technique to sample the posterior probability density function (PDF) of the model parameters.

The magnification factor, μ , is calculated as the ratio between the total flux density of the sources, as measured in the SP within the region of signal-to-noise ratio $\text{SNR} \geq 3$, and the flux density of the corresponding image in the IP. The uncertainty on the magnification factor is derived by computing μ 1000 times, perturbing each time the lens model parameters around their best-fitting values.

The modeling is carried out on the reduced ACS + F606w image, with a pixel scale of $0.06''$. A noise map is constructed from the provided weight map and the psf is obtained by median combining 3 unsaturated stars in the vicinity of the target. The lens is subtracted from the image after fitting its light profile with GALFIT ([Peng et al. 2002](#)).

The best-fitting SIE model has $\theta_E = 0.76_{-0.01}^{+0.02}$ arcseconds, $q_L = 0.66_{-0.06}^{+0.04}$, and $\theta_L = -35.6_{-0.8}^{+0.6}$ degrees, with an external shear of strength $\gamma = 0.31_{-0.02}^{+0.01}$ and angle $\theta_\gamma = -34.9_{-0.7}^{+0.6}$ degrees. The estimated Einstein radius can be converted into a velocity dispersion, σ_{SIE} , using the relation

$$\theta_E = 4\pi \left(\frac{\sigma_{\text{SIE}}}{c} \right)^2 \frac{D_{\text{LS}}}{D_{\text{S}}}, \quad (1)$$

where D_{LS} and D_{S} are the angular-diameter distances from lens to source and observer to source, respectively. We find $\sigma_{\text{SIE}} = 197.9_{-1.3}^{+2.6} \text{ km s}^{-1}$, in good agreement with the value derived from the line profile.

The results of the lens modeling are shown in Fig. 6. The reconstructed source, in the rightmost panel, is compact. This result is not surprising, as there is no evidence of extended structure in the lensed images. The estimated magnification factor is $\mu = 4.5_{-0.8}^{+1.0}$.

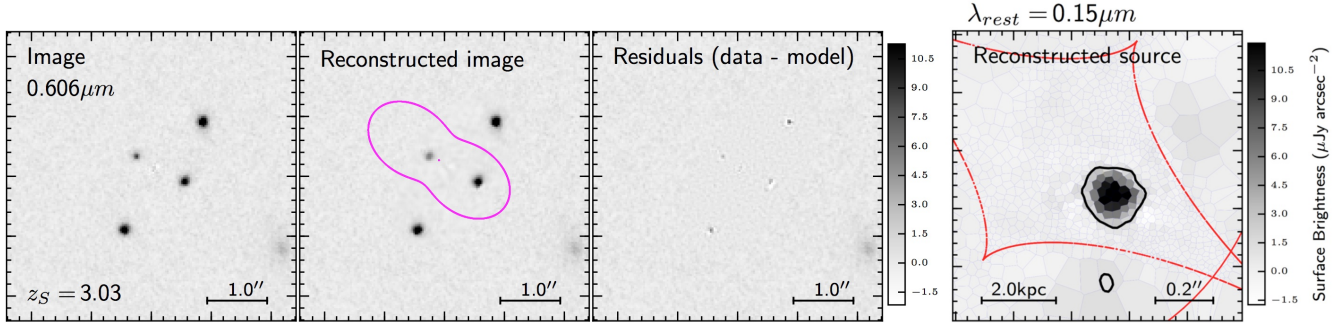


Figure 6. Results of the lens modeling showing, from left to right, the input image, the reconstructed image, the residuals and the reconstructed source. The purple curve in the second panel from the left is the tangential critical line, while the red curves in the rightmost panel are the caustics.

4. SUMMARY AND CONCLUSIONS

We presented the spectroscopic confirmation of a new gravitational lens J2211 –0350 with Einstein cross configuration discovered inspecting RELICS images. The lens is an elliptical galaxy ($M_V \sim -21$) at $z = 0.556$ while the lensed source is a Ly-break galaxy at $z = 3.03$. Modeling of the lens shows that the Einstein cross is well reproduced by a SIE model with Einstein ring of 0.76 arcsec and that includes the shear effect due to the foreground massive low redshift cluster of galaxies. The lensed source is magnified by a factor 4.5. This gravitational lens is similar to the case reported by Bolton et al. (2006) for J1011 +0143. This is the second case of an Einstein cross gravitational lens produced by a distant Ly-break galaxy. The intrinsic Ly α luminosity, taking into account the magnification factor, is $L(\text{Ly}\alpha) = 5 \times 10^{42} \text{ erg s}^{-1}$, a factor ~ 2 higher than that found

by Bolton et al. (2006) for J1011 +0143. The Ly α luminosity is close to L^* of the Luminosity Function of high redshift Ly α emitters (see e.g. Sobral et al. 2018).

We thank Mario Radovich, Simona Paiano and Aldo Treves for useful discussions. Based on observations made with the GTC telescope, in the Spanish Observatorio del Roque de los Muchachos of the Instituto de Astrofísica de Canarias, under Director’s Discretionary Time. This work is based on observations taken by the RELICS Treasury Program (GO 14096) with the NASA/ESA HST, which is operated by the Association of Universities for Research in Astronomy, Inc., under NASA contract NAS5-26555.

Facilities: GTC(OSIRIS), HST(ACS), HST(WFC2)

REFERENCES

- Agnello A., et al., 2018b, MNRAS, 475, 2086
 Bolton, A. S., Moustakas, L. A., Stern, D., et al. 2006, ApJL, 646, L45
 Bonvin, V., Courbin, F., Suyu, S. H., et al. MNRAS, 465, 4914
 Cepa, J., Aguiar-Gonzalez, M., Bland-Hawthorn, J., et al. 2003, in Proc. SPIE, Vol. 4841, 1739
 Cappellari, M. & Emsellem, E. 2004, PASP, 116, 138
 Cerny C., et al., 2018, ApJ, 859, 159
 Enia, A. et al., 2018, MNRAS, 475, 3467
 Jacoby G. H., Hunter D. A., Christian C. A., 1984, ApJS, 56, 257
 Jones, T., Stark, D. P., & Ellis, R. S. 2012, ApJ, 751, 51
 Morgan N. D., Caldwell J. A. R., Schechter P. L., Dressler A., Egami E., Rix H.-W., AJ, 127, 2617
 Nightingale, J. W. & Dye, S. MNRAS, 452, 2940
 Oguri M., Marshall P. J., 2010, MNRAS, 405, 2579
 Paterno-Mahler et al. ApJ, 863, 154
 Peng, C. Y., Ho, L. C., Impey, C. D., & Rix, H.-W. 2002, AJ, 124, 266
 Schechter P. L., Morgan N. D., Chehade B., Metcalfe N., Shanks T., McDonald M., 2017, AJ, 153, 219
 Suyu, S. H., Marshall, P. J., Hobson, M. P. & Blandford, R. D., 2006, MNRAS, 371, 983
 Suyu S. H. et al., 2014, ApJ, 788, L35
 Suyu, S. H., Bonvin, V., Courbin, F., et al. 2017, MNRAS, 468, 2590
 Salmon B., et al., 2017, arXiv, arXiv:1710.08930
 Salmon, et al. ApJ, 864, 22
 Sobral, S. S. et al. 2018 MNRAS, 476, 4725
 Treu, T. 2010, ARA&A, 48, 87
 Treu T., Koopmans L. V. E. MNRAS, 337, 2006
 Treu T., Koopmans L. V. E., ApJ, 611, 739
 Warren, S. J. & Dye, S. 2003, MNRAS, 590, 673
 Williams P., Agnello A., Treu T., 2017, MNRAS, 466, 3088
 Williams P. R., et al., 2018, MNRAS, 477, L70

Vazdekis, A., Ricciardelli, E., Cenarro, A. J., et al. 2012,
MNRAS, 424, 157

Wisotzki L., Schechter P. L., Bradt H. V., Heinmuller J.,
Reimers D., A&A,395, 17